Applied Physics A (2023) 129:414
https://doi.org/10.1007/s00339-023-06694-y

Applied Physics A
Materials Science & Processing

Optimization of annealing temperature on the formation CZTSe absorber layer

Vishvas Kumar[1] · **Udai P. Singh**[2]

Received: 19 January 2023 / Accepted: 3 May 2023 / Published online: 13 May 2023

Abstract
In the present work, we studied the optimization of annealing temperature on the formation of $Cu_2ZnSnSe_4$ (CZTSe) thin films and its impact on the film properties. The CZTSe films were deposited on Mo/SLG substrate by the thermal evaporation method. All the elements of the compound were deposited in the stack using its pellets. After the successful deposition of the films, the composition of the as deposited film was measured, then it was proceeded further for two steps annealing. The annealing parameter is one of the crucial steps for obtaining good quality kesterite-based absorber layer. In the present work, we have utilized two-step annealing to achieve the absorber layer suitable for device fabrication. The annealing in Se atmosphere were carried out at 230 °C for 10 min in first step followed by another 10 min annealing in second step with a temperature variation from 430 to 490 °C. The final temperature was varied to investigate the influence of annealing temperature on the absorber layer (CZTSe) film properties and its optimization. The films annealed between 470 and 490 °C are showing better structural, optical, electrical and morphological properties for further processing.

Keywords CZTSe · Thermal evaporation · Stack deposition · Rapid thermal processing

1 Introduction

CZTS/Se is a kesterite-based p-type direct bandgap semiconductor compound. Its constituent elements (Cu, Zn, Sn, S/Se) are abundant in earth crust which is less toxic [1]. The bandgap range of CZTS/Se is from 1 to 1.5 eV according to the S/Se ratio. Its absorption coefficient is greater than 10^4 cm^{-1} and flexible with the deposition technique. All these properties make CZTS/Se as one of the suitable materials for solar cell absorber layer. Until now, maximum efficiency achieved is around 12.6% which is far below its theoretical efficiency (33.7%) [2]. Hence, many researchers started focusing on kesterite material and studied its different parameters such as deposition technique, annealing parameters, compositional variation, and surface morphology to overcome the limited efficiency. The deposition techniques highly affect its surface morphology and adherence on the substrate. The researchers have used different both vacuum and non-vacuum techniques to deposit CZTS/Se film such as thermal evaporation [3], magnetron sputtering [4] and ion beam deposition [5], screen-printing [6], spin coating [7], and spray pyrolysis [8] etc. In this work, thermal evaporation technique is used for the deposition of the CZTSe as it provides better adherence, uniformity and surface morphology [9]. During annealing of CZTSe, Sn and Se loss is observed which effects the compositional ratio and crystal growth of the films which in turn deteriorates the device performance. The stack deposition prevents the loss of elements and provides better composition of the films [10].

After deposition of the Cu, Zn, Sn and Se using thermal evaporation and confirming the desired compositional ratio, annealing is carried out in the next step to form the CZTS/Se compound. Variation in annealing temperature affects the properties of the films. The two-step annealing process improves the grain growth and reduces the pinholes as compared to single step annealing in Se atmosphere [11].

Teoman Özdal et al. [12] prepared the CZTS film using Spin coating and annealed at 300 °C, 500 °C and 550 °C using one step and studied the Morphology and Optoelectronics Properties. Altowairqi et al. [13] prepared CZTS

✉ Udai P. Singh
singhup@kiit.ac.in

[1] School of Engineering and Technology, CMR University, Bengaluru 562149, India

[2] Thin Film Photovoltaic Lab, School of Electronics Engineering, Kalinga Institute of Industrial Technology (Deemed to be University), Bhubaneswar 751024, India

films using spin coating of nanocrystal ink and annealed at 500 °C for 1 h with a ramping rate of 10 °C/min under $H_2S + N_2$ atmosphere and studied the effect of temperature, time, ramping rate and atmosphere on the properties of CZTS films. Simya et al. prepared CZTSe and CZTS film by a multicomponent single target with different RF sputter powers and a constant annealing temperature of 450 °C they investigated the structural, optical and electrical properties. They reported an efficiency of 3.72% and 2.6% for the CZTSe and CZTS films, respectively [14]. After covering through different literature, it is observed that there is no optimized annealing temperature for the formation of pure phase of CZTSe compound.

In the present work, films were deposited using thermal evaporation method in stack format (CuSn/Zn/Se/CuSn/Se). Post deposition annealing was carried out in two steps, first step is constant at 230 °C for 10 min for all the films and in the second step the temperature was varied between 430 and 490 °C with 20 °C temperature difference for 10 min duration (Fig. 1) using rapid thermal processing (RTP). The effect of two-step selenization temperature on the structural, optical and electrical properties of CZTSe films prepared in stacks by thermal evaporation were studied.

2 Experimental technique

Soda lime glass (SLG) substrates were ultrasonically cleaned in a soap solution followed by 10 min in propanol. After cleaning, the SLG was dried by blowing N_2 gas. Then, the Mo was deposited in a two-step process on the SLG substrate having a thickness of about 830 nm. In the first step, the deposition was carried out at low Argon (20 Standard cubic centimeter (SCCM)) flow rate and high (240 W) power for 40 min and in the second step, high Argon (40 SCCM) flow rate and low Power (120W) for 40 min has been used to increase the adherence and reduce the pinholes. During the deposition the chamber pressure was maintained at around 10^{-3} mbar. After optimization of compositional ratio, the constituent elements of CZTSe were deposited in a stack as; CuSn/Zn/Se/CuSn/Se using thermal evaporation on Mo deposited SLG. The obtained film thickness was around 1.52 µm. For deposition, pellets of individual elements and/or compound with 99.99% of purity were placed in the Tungsten helical boat in proper ratio to achieve the desired composition. When chamber pressure reached at 10^{-6} mbar then power supply (up to 50 W) provided to the helical boat for deposition. Post-deposition annealing was carried out in two steps, first step is constant at 230 °C for 10 min and second step was varied from 430 to 490 °C with 20 °C temperature difference for 10 min (Fig. 1) using rapid thermal processing (RTP). For annealing/selenization, along with the films, 0.2 g of Se shot was put separately in the graphite box and the graphite box was placed in the middle of the annealing chamber. The annealing chamber pressure was maintained at 10^{-3} mbar. According to the variation of annealing temperature in the second step, the films were named as C1(430 °C), C2(450 °C), C3(470 °C) and C4(490 °C), respectively, and the variation done during annealing with respect time is shown in Fig. 1.

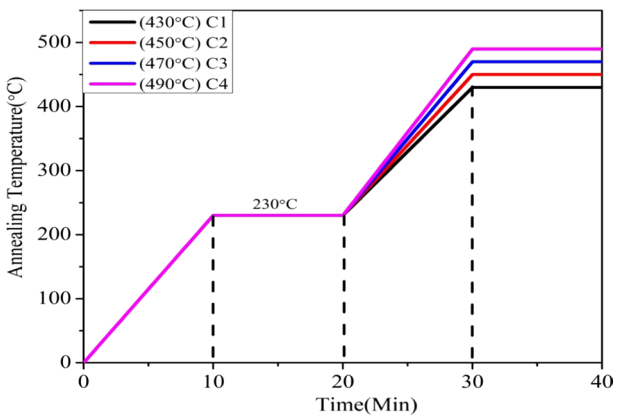

Fig. 1 Variation in annealing temperature of the films

3 Characterization

The X-ray diffractometry (XRD) (Shimadzu-6100) with Cu-Kα radiation of λ = 1.54 Å was employed to ascertain the phases of the CZTSe film. The EDXRF (Shimadzu EDX-7000) was used for compositional analysis and thickness measurement. The EDXRF was calibrated against the standard sample provided by Shimadzu EDX-7000. Surface morphology analysis was carried out using Scanning Electron Microscopy (SEM) (Gemini 500) technique to observe the surface properties after annealing. The UV–Vis spectrophotometer (Shimadzu UV-2450) was used to find the bandgap of the film. The Hall measurement system (HMS-3000) at room temperature was utilized to measure the Electrical properties viz. Carrier conc., mobility, resistivity and conductivity of the films.

4 Results and discussion

4.1 Structural analysis of the films

The XRD pattern of the annealed films is shown in Fig. 2. From the XRD pattern; multiple peaks of CZTSe are observed in the films which confirms that CZTSe is polycrystalline in nature. The main peak of CZTSe is observed around the $2\theta = 26.91°$ (JCPDS no. 52-0868). To further investigate the main peak, the peaks were deconvoluted

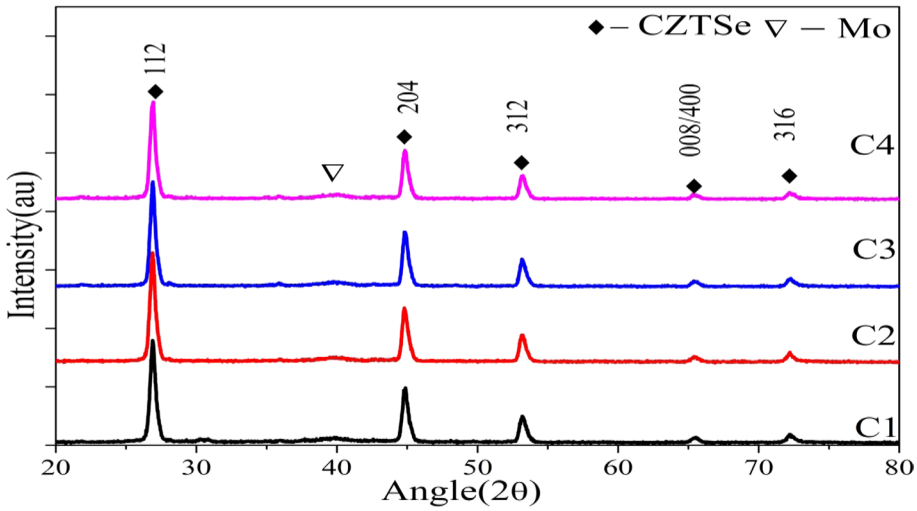

Fig. 2 XRD pattern of the films

(Fig. 3) using Gaussian peak fit. Two additional peaks of ZnSe (JCPDS No – 89-2940) and $SnSe_2$ (JCPDS No-89-3917) are observed for sample C1 and C2 and these peaks disappeared for sample C3 and C4 (Fig. 3). This may be possibly due to the annealing, which allows the faster grain growth and recrystallization in the films. Annealing through RTP releases internal stress in the films, which leads to deformation, and distortion in the crystal lattice. According to Jianjun Li et al. [15], if ZnSe exists in the film, it may be on the front surface of the CZTSe layer and it reduces the interfacial recombination and dislocation between CZTSe/CdS interface. When particle size and strain vary irregularly with 2θ, then strain and crystallite size can be estimated using Williamson–Hall (W–H) Eq. (1) as we know that peak broadening in the XRD peak is due to instrument and sample. After subtracting the contribution from the instrument, broadening due to sample is mainly due to the crystallite size and micro-strain.

$$\beta = \beta_{\text{crystallite size}} + \beta_{\text{micro strain}},$$

$$\beta = +4\varepsilon \tan\theta.$$

Multiply both sides by cosθ,

$$\beta\cos\theta = 4\varepsilon\sin\theta + \frac{k\lambda}{D}, \tag{1}$$

where k is constant and it is value is 0.94 by presuming spherical nature of powder, 'β' is the FWHM of the peaks, 'ε' is the strain and can be obtained from the slope of the W–H plot, and 'D' is the average crystallite size determined from the inverse of the intercept.

The Dislocation density (δ) can be estimated using Eq. (2)

$$\delta = 1/\,\mathrm{D}^2. \tag{2}$$

Employing the Bragg's equation, the spacing between crystals can be calculated using Eq. (3):

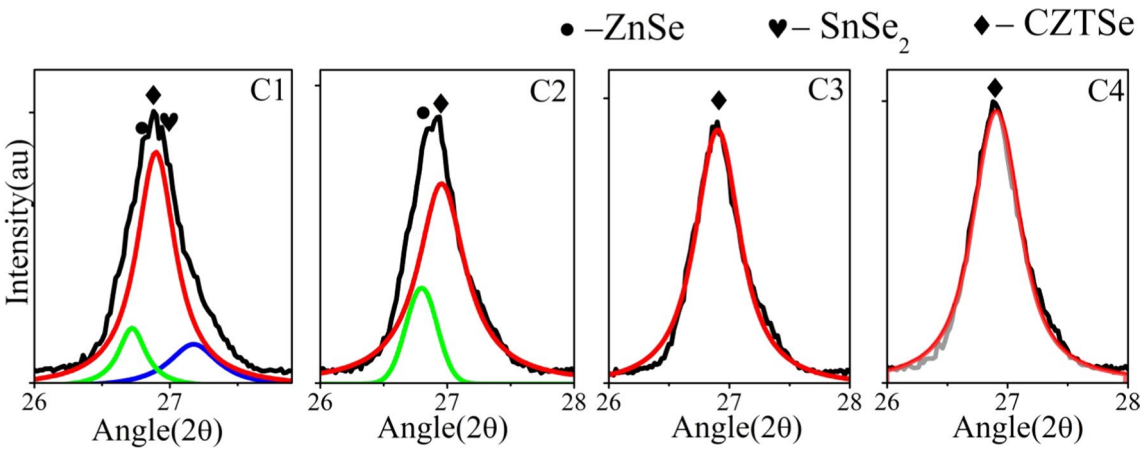

Fig. 3 Deconvoluted main peaks of all the films (red curve is for CZTSe, green is for ZnSe and blue is for $SnSe_2$)

$$d = n\lambda/2\sin(\theta), \tag{3}$$

where n is diffraction order (generally $n = 1$).

The lattice constant (a, b, c) of CZTSe which corresponds to a tetragonal BCC structure can be estimated using equation [16]

$$1/d^2 = \left(h^2 + K^2\right)/a^2 + l^2/c^2, \tag{4}$$

where 'd' stands for the crystal spacing, h, k and l stands for miller indices.

The crystallite size was found to increase with the increase in annealing temperature. The strain and crystallite size calculated using the W–H plot are shown in Table 1. The W–H plot shows the positive slope which indicates the presence of tensile strain in the films as shown in Fig. 4. Annealing of the sample leads to a decrease in micro strain and dislocation density and an increase in crystallite size, which is from 20.72 to 22.08 nm for the film C1 to C4 [17]. The dislocation density of the CZTSe thin-film decreases with the increase in the annealing temperature, which may be due to the relaxation of the built-up strain generated during the deposition of the film. This phenomenon is consistent with previous studies [9, 10]. The increase in the crystallite size with annealing temperature may be associated with the coalescence of smaller particles to form larger clusters due to a reduction in the lattice strain. The lattice parameters $a = b$ is almost constant for all the films but with increases in annealing temperature c parameters of the film gradually increases. Thus, the volume of the unit cell is also increases gradually with annealing temperature. But c/2a ratio is near to one shows the pure kesterite phase formation in the film (Table 2). Here, it is observed that with increase in annealing temperature, crystallite size increases which in turn induces an expansion in lattice parameter of unit cell and reduction in the lattice strain values [18].

4.2 Compositional analysis

The composition and thickness of the films measured using Shimadzu EDXRF-7000 in the air environment are shown in Table 3. From the table it is confirmed that the films are Cu poor and Zn rich which is suitable for solar cell application. Generally, Cu rich films give higher electrical conductivity to the CZTSe compound resulting in shunt losses which eventually leads to reduced solar cell performance [19]. When compared with as deposited film, Cu and Sn at% decreases after but Se at% increases due to annealing in the presence of Se atmosphere. The Cu/(Zn + Sn) is almost constant but Zn/Sn ratio is increasing due to loss of Cu and Zn after annealing. All the films (C1-C4) have Cu/(Zn + Sn) < 1,Zn/Sn > 1 and Se/Metal ≅ 1 as required for the good absorber layer. The thickness of the annealed films are around 1.73 µm.

Table 1 Micro-strain, avg. crystallite size of the films from the Williamson–Hall equation

Parameters		Peak position	FWHM	X-axis	Y-axis	Intercept	Crystallite Size	Slope	Micro strain (ε)	Dislocation density (δ)
K	λ (Å)	2θ (°)	β (°)	$4\sin\theta$	$\beta\cos\theta$	$C = \frac{K\lambda}{D}$	$D(nm)$	m	$\times 10^{-3}$	$\times 10^{-3}$ nm^{-2}
C1										
0.94	1.5406	26.88	0.48	0.93	8.15×10^{-3}	0.00699	20.72	0.00107	1.07	2.32
		44.84	0.51	1.53	8.23×10^{-3}					
		53.24	0.58	1.79	9.05×10^{-3}					
		65.49	0.64	2.16	9.40×10^{-3}					
C2										
0.94	1.5406	26.89	0.47	0.93	7.98×10^{-3}	0.00684	21.17	0.00101	1.01	2.23
		44.86	0.5	1.53	8.07×10^{-3}					
		53.22	0.55	1.79	8.58×10^{-3}					
		65.47	0.63	2.16	9.25×10^{-3}					
C3										
0.94	1.5406	26.9	0.46	0.93	7.81×10^{-3}	0.00661	21.91	0.00098	0.98	2.08
		44.88	0.48	1.53	7.74×10^{-3}					
		53.24	0.53	1.79	8.27×10^{-3}					
		65.49	0.62	2.16	9.10×10^{-3}					
C4										
0.94	1.5406	26.9	0.46	0.93	7.81×10^{-3}	0.00656	22.08	0.00092	0.92	2.05
		44.87	0.45	1.53	7.26×10^{-3}					
		53.24	0.52	1.79	8.11×10^{-3}					
		65.48	0.61	2.16	8.96×10^{-3}					

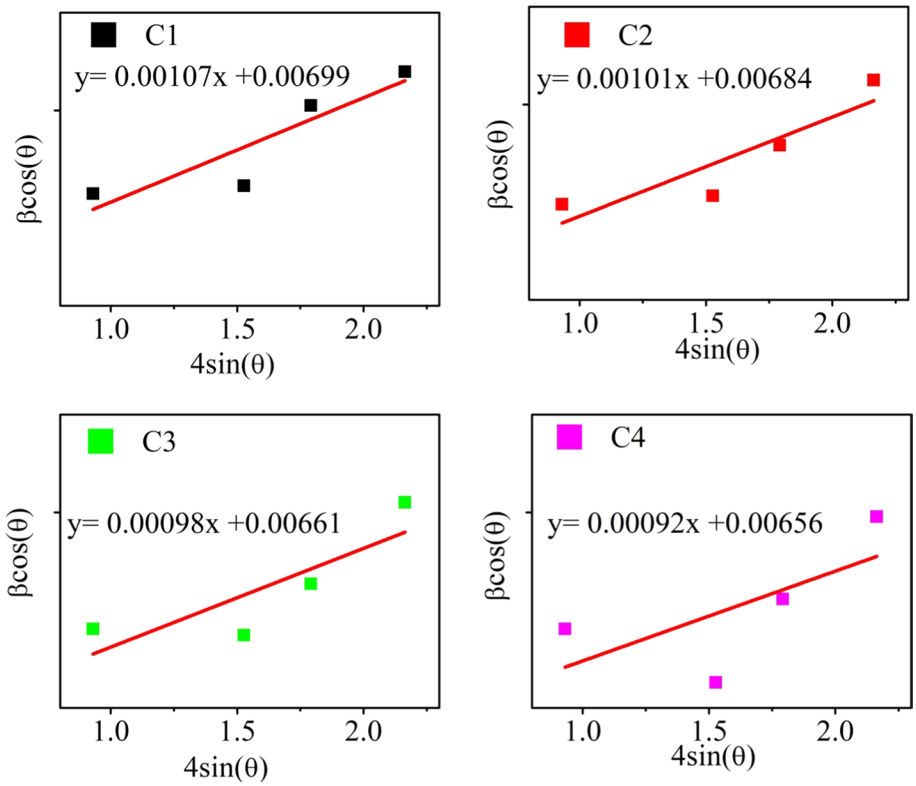

Fig. 4 Williamson–Hall plots of the films

Table 2 Lattice parameter of the films

Sample name	$a=b$(Å)	c(Å)	$c/2a$	Volume (Å)^3
JCPDS-52-0868	5.69	11.33	0.99	366.82
C1	5.70	11.44	1.00	371.68
C2	5.70	11.51	1.00	373.95
C3	5.70	11.63	1.02	377.85
C4	5.70	11.64	1.02	378.18

4.3 Surface morphology

The Surface morphology analysis has been carried using the Scanning Electron Microscopy technique, to study the grain growth and its surface behavior. Morphologies of post annealed sample through SEM are shown in Fig. 5. In film C1, agglomerated layer observed on the surface and the grains are very small. When second step annealing temperature increases to 450˚C these agglomerated layers removed from the surface and grain size slightly increases but cracks were also observed. This might be due presence of binary phase in the film C1 and C2. Further increase in annealing for the film C3 and C4, grain size is improved which can be observed on the surface of the film. It is also found that the surface of the films is more uniform as compared to C1 and C2 films. The large grain size is very important for reducing the grain boundaries and charge trapping in the CZTSe film.

4.4 Optical properties

To study the optical properties of the film, absorption and reflectance were measured using Shimadzu UV–Vis 2450. From absorption curve of the films, band gap is calculated using Tauc formula 5 and 6.

Table 3 Composition of the films

Sample name	Cu (at %)	Zn (at%)	Sn (at%)	Se (at%)	Cu/(Zn + Sn)	Zn/Sn	Se/metal	Thickness (um)
As-deposited	23.70	16.08	15.07	45.15	0.76	1.06	0.82	1.61
C1	21.90	16.06	13.50	48.52	0.74	1.18	0.94	1.73
C2	21.86	15.98	13.52	48.63	0.74	1.18	0.95	1.76
C3	21.65	16.45	12.73	49.15	0.74	1.29	0.97	1.74
C4	22.15	16.48	12.11	49.25	0.77	1.36	0.97	1.71

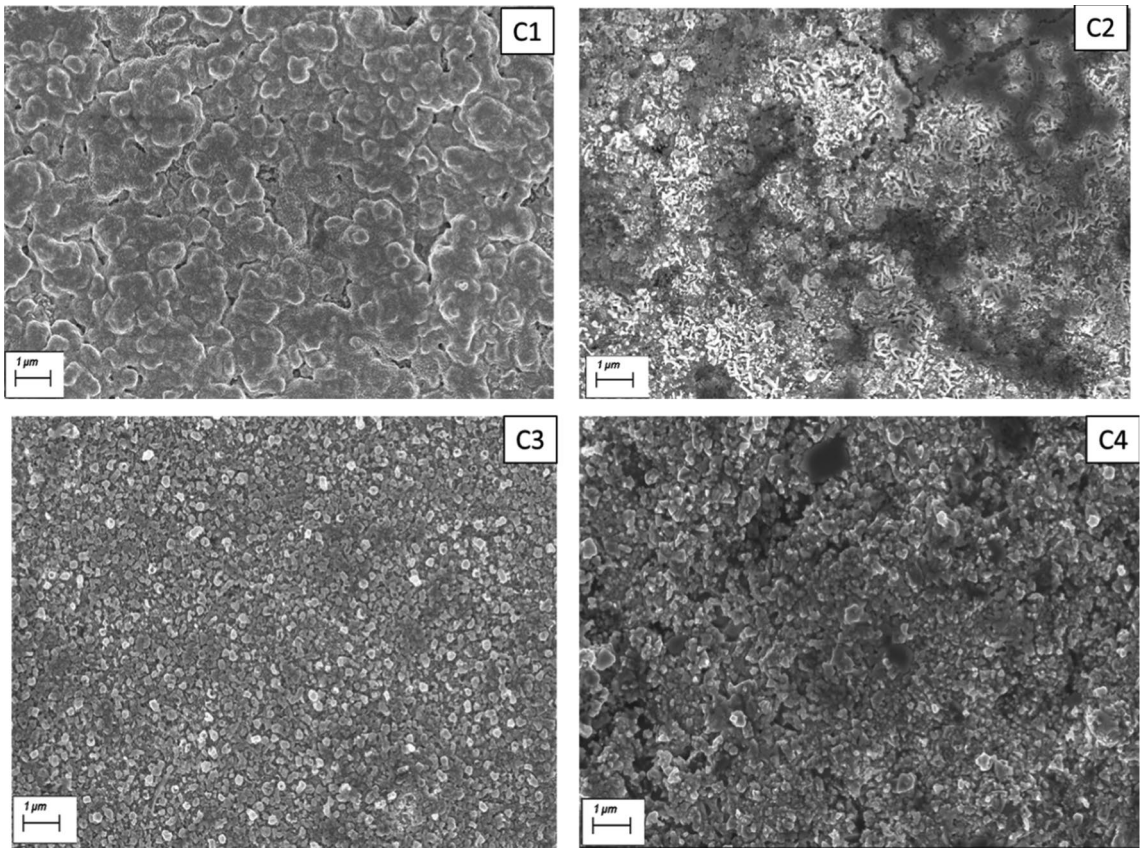

Fig. 5 Surface morphology of the films

$$(\alpha h\upsilon)^n = K(h\upsilon - Eg), \tag{5}$$

$$\alpha = (2.303 \times A)/T, \tag{6}$$

where 'α' stands for absorption coefficient, 'A' stands for absorbance, 'T' stands for thickness of the film, 'K' is a constant and n stands for transition class process. The value of n is 2 and 0.5 for direct band gap and indirect band gap respectively. The CZTSe band gap is estimated by extrapolating the slope of $(\alpha h\upsilon)^2$ to the $(h\upsilon)$ axis (Fig. 8). The absorption of the films increases slightly with increase in annealing temperature and in the middle of the visible region (380–700 nm) absorption is maximum in all the film as shown in Fig. 6. The reflectance of the films C1, C2 and C3 increases with increase in annealing temperature but in C3 and C4 films it is almost constant (Fig. 6) may be due to variation in composition after annealing. The absorption coefficient curve of the films shows that its value is greater than 10^4 cm^{-1} in all the film and it also increases with the increase of annealing temperature which may be due to the improvement in crystallinity and grain growth (Fig. 7).

The band gap plot of the films are shown in the Fig. 8. With the increase in annealing temperature, there is fraction of change in the band gap of the films which can be observed. A fractional reduction in the band gap from 1.35 to 1.33 eV may be due to variation in the film composition or improvement in crystallite size after annealing. When crystallite size increases boundary between crystals decreases so that carrier recombination decreases which in turn increase the conductivity and decreases the bandgap.

4.5 Electrical properties

Electrical properties of the films are measured using Hall Effect measurement system at room temperature and the obtained results are shown in Table 4. The carrier concentration of all the films is in the order of 10^{18} $cm^{-3.}$ With the increase in annealing temperature the mobility and conductivity of the film increases. This may be possible due to the increase in the grain size. Increase in mobility subsequently reduces the device series resistance and improves the performance of CZTSe based solar cell [20].Increase in conductivity of the CZTSe absorber layer is due to the decrease in grain boundary and increase in carrier lifetime. The I–V plot of the film for the calculation of sheet resistance is shown in Fig. 9. The sheet resistance of the film decreases with increase in annealing temperature. But the film which were

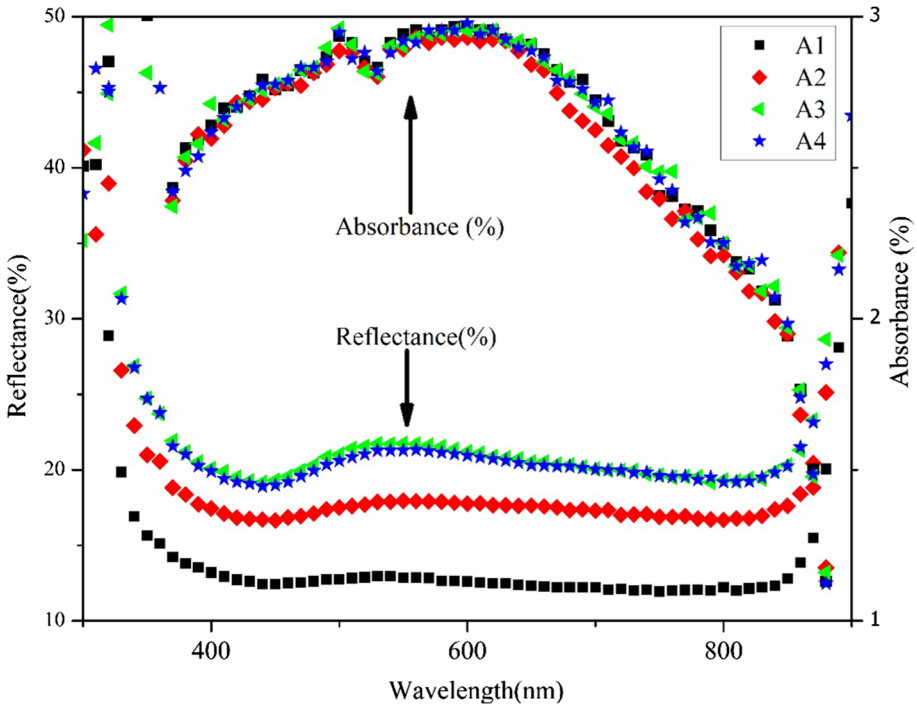

Fig. 6 Reflectance and absorbance plot of the films

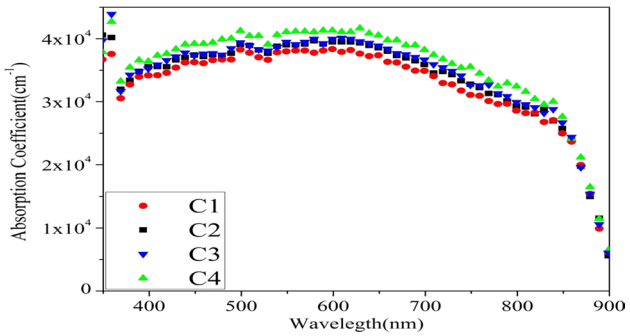

Fig. 7 Absorption coefficient of the films

annealed at 470 °C(C3) and 490 °C(C4) the curve of the sheet resistance almost overlapping which indicates slight variation in the sheet resistance (Table 4). The sheet resistance is high but conductivity and carrier concentration is low may be due to Cu poor in the films.

5 Conclusion

We have studied the properties of CZTSe thin film absorber layer fabricated in stacks through thermal evaporation process. The effect of selenization temperature on the structural, surface morphology, electrical and optical properties of the CZTSe films was examined. Polycrystalline CZTSe thin films with kesterite crystal structure were obtained in all the films. Binary phases (ZnSe and $SnSe_2$) observed in C1, and C2 film, which is suppressed in C3 and C4 with increase in selenization temperature. The crystallite size of the films are also increased in the order to C1 < C2 < C3 < C4 with the increase in selenization temperature. From the surface morphology study, it is observed that the films are more uniform and have large grain size when selenization temperature increased from 430 to 490 °C. EDXRF analysis reveals that stoichiometric composition of the constituent elements in all the films. UV analysis shows that the band gap of the film decreases when selenization temperature increases which is due to the increase in crystallite size. The carrier concentration, mobility of the films increases and sheet resistance and resistivity of the films decreases due to variation in selenization temperature.

The most promising condition to get good quality absorber layer is 230 °C for 10 min followed by 470 °C or 490 °C for 10 min. The studies shows that the films C3 and C4 has better structural, optical, electrical and morphological properties which is suitable for solar cell device application. This study reveals the importance of selenization temperature on the formation of CZTSe phase, improvement of crystal structure, electrical properties, surface morphology and tuning of band gap for better performance of solar cell application.

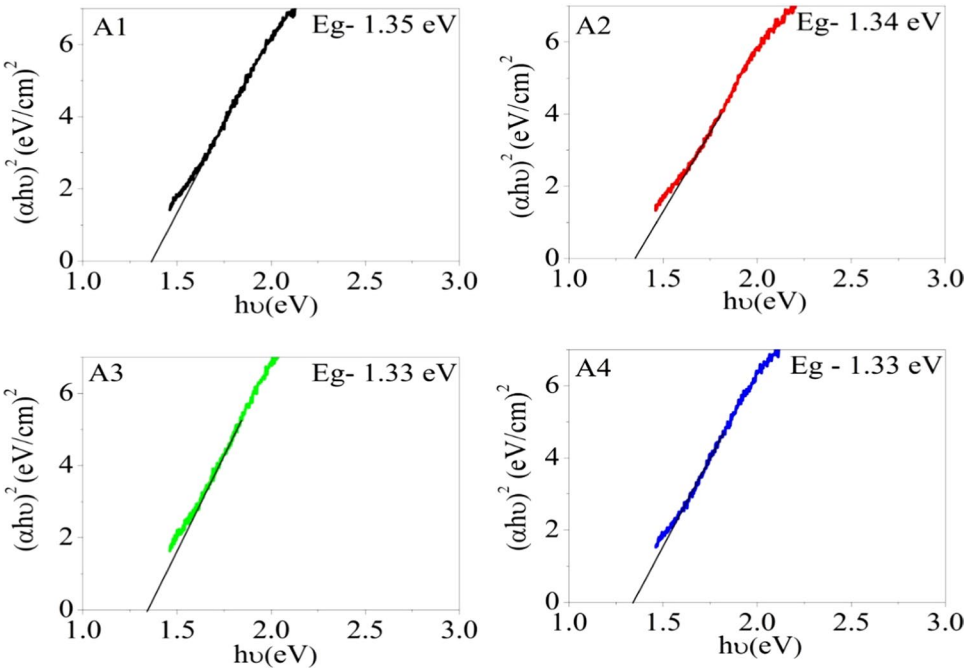

Fig. 8 Band gap plot of the films

Table 4 Electrical properties of the films

Sample name	Carrier Conc. (cm^{-3})	Mobility ($cm^2V^{-1}S^{-1}$)	Conductivity ($S.cm^{-1}$)	Resistivity (Ω.cm)	Sheet resistance (Ω)
C1	7.24×10^{18}	4.49	5.21	19.2×10^{-2}	1109.83
C2	4.06×10^{18}	8.12	5.28	18.9×10^{-2}	1073.86
C3	2.69×10^{18}	12.68	5.47	18.2×10^{-2}	1045.98
C4	2.64×10^{18}	13.27	5.62	17.8×10^{-2}	1040.94

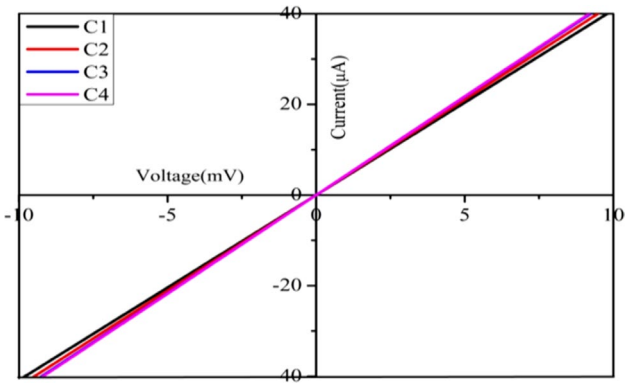

Fig. 9 I–V plot of the films for sheet resistance calculation

Acknowledgements The authors are thankful to the DST_SERB, New Delhi for the financial assistance under Grant # CRG/2022/003593.

Data availability Data can be made available on request.

Declarations

Conflict of interest The authors declared that there is no conflict of interest

Human research and animal participants There is no involvement of Human Participants and/or Animals in this research.

References

1. V. Kumar, U.P. Singh, Formation of CZTSSe absorber layer using thiourea treatment of CZTSe. Mater. Today **39**, 1838–1842 (2021)
2. W. Wang, M.T. Winkler, O. Gunawan, T. Gokmen, T.K. Todorov, Y. Zhu, D.B. Mitzi, Device characteristics of CZTSSe thin-film solar cells with 12.6% efficiency. Adv. Energy Mater. **4**, 1301465 (2013)
3. S. Padhy, V. Kumar, N.B. Chaure, U.P. Singh, Impact of germanium nano layer on the CZTSe absorber layer properties. Mater. Sci. Semicond. Process. **138**, 106276 (2022)
4. O.K. Simya, B. Geetha-Priyadarshini, K. Balachander, A.M. Ashok, Formation of a phase pure kesterite CZTSe thin films

using multisource hybrid physical vapour deposition. Mater. Res. Express **7**, 016419 (2020)
5. J. Zhao, G. Liang, Y. Zeng, P. Fan, Hu. Juguang, J. Luo, D. Zhang, The influence of sequence of precursor films on CZTSe thin films prepared by ion-beam sputtering deposition. J. Semicond. **38**, 023002 (2017)
6. V. Kumar, S. Padhy, A. Basak, U.P. Singh, Effect of HCl and NH_4OH etching on CZTSSe absorber layer. Vacuum **155**, 336–338 (2018)
7. G.M. Ilari, M. Carolin, F. Carmen, Z. Alexander, R.U. Yaroslav, E. Romanyuk, A.N. Tiwari, $Cu_2ZnSnSe_4$ solar cell absorbers spin-coated from amine-containing ether solutions. Solar Energy Mater. Solar Cells **104**, 125–130 (2012)
8. X. Zeng, K.F. Tai, T. Zhang, L.H. Wong, $Cu_2ZnSn(S, Se)_4$ kesterite solar cell with 51% efficiency using spray pyrolysis of aqueous precursor solution followed by selenization. Solar Energy Mater. Solar Cells **124**, 55–60 (2014)
9. V. Kumar, A. Dutta, UP Singh Optimization of selenization parameters for fabrication of CZTSe thin film. Superlattices Microstruct. **144**, 106578 (2020)
10. V. Kumar, U.P. Singh, Effect of selenization temperature on the formation of CZTSe absorber layer. Appl. Phys. A **125**, 1–8 (2019)
11. V. Kumar, U.P. Singh, Effect of temperature profile on the formation of CZTSe absorber layer, *47th IEEE Photovoltaic Specialists Conference* (PVSC), 0309–0313 (2021)
12. T. Özdal, T. Chtouki, H. Kavak et al., Effect of annealing temperature on morphology and optoelectronics properties of spin-coated CZTS thin films. J. Inorg. Organomet. Polym. **31**, 89–99 (2021)
13. Y. Altowairqi, A. Alsubaie, K.P. Stroh, I.G. Perez-Marin, L. Bowen, M. Szablewski, D.P. Halliday, The effect of annealing conditions: temperature, time, ramping rate and atmosphere on nanocrystal Cu_2ZnSnS_4 (CZTS) thin film solar cell properties. Mater. Today: Proc. **18**, 473–486 (2019)
14. O.K. Simya, T. Vijayaraghavan, B. Subramanian, A.M. Ashok, Effect of RF sputter power on deposition of CZTX (X=S, Se) active layer without selenization/sulfurization, for solar cell applications. J. Alloys. Compound **898**, 162838 (2022)
15. J. Li, J. Huang, F. Ma, H. Sun and X. Hao, Unveiling microscopic carrier loss mechanisms in 12% efficient $Cu_2ZnSnSe_4$ solar cells. Nat. Energy 1078-7 (2022)
16. J. Henry, K. Mohanraj, G. Sivakumar, Photoelectrochemical cell performances of $Cu_2ZnSnSe_4$ thin films deposited on various conductive substrates. Vacuum **156**, 172–180 (2018)
17. P.M. Shafi, A.C. Bose, Impact of crystalline defects and size on X-ray line broadening: a phenomenological approach for tetragonal SnO_2 nanocrystals. AIPAdv. **5**, 5 (2015)
18. A.B. Andrade, N.S. Ferreira, M.E.G. Valerio, Particle size effects on structural and optical properties of BaF_2 nanoparticles. RSC Adv. **7**, 26839–26848 (2017)
19. D.S. Dhawale, A. Ali, A.C. Lokhande, Impact of various dopant elements on the properties of Kesterite compound for solar cell application: a status review. Sustain. Energy Fuels **3**, 1365–1383 (2019)
20. C.-C. Tseng, G. Wu, L.-B. Chang, M.-J. Jeng, W.-S. Feng, D.W. Chen, L.-C. Chen, K.-L. Lee, Effects of annealing on characteristics of $Cu_2ZnSnSe_4/CH_3NH_3PbI_3$/ZnS/IZO nanostructures for enhanced photovoltaic solar cells. Nanomaterial's **10**, 521 (2020)